HEALTH AND MEDICINE

Heparin-mediated delivery of bone morphogenetic protein-2 improves spatial localization of bone regeneration

Marian H. Hettiaratchi[1,2], Laxminarayanan Krishnan[1], Tel Rouse[1], Catherine Chou[1], Todd C. McDevitt[3,4], Robert E. Guldberg[1,2]*

Supraphysiologic doses of bone morphogenetic protein-2 (BMP-2) are used clinically to promote bone formation in fracture nonunions, large bone defects, and spinal fusion. However, abnormal bone formation (i.e., heterotopic ossification) caused by rapid BMP-2 release from conventional collagen sponge scaffolds is a serious complication. We leveraged the strong affinity interactions between heparin microparticles (HMPs) and BMP-2 to improve protein delivery to bone defects. We first developed a computational model to investigate BMP-2–HMP interactions and demonstrated improved in vivo BMP-2 retention using HMPs. We then evaluated BMP-2–loaded HMPs as a treatment strategy for healing critically sized femoral defects in a rat model that displays heterotopic ossification with clinical BMP-2 doses (0.12 mg/kg body weight). HMPs increased BMP-2 retention in vivo, improving spatial localization of bone formation in large bone defects and reducing heterotopic ossification. Thus, HMPs provide a promising opportunity to improve the safety profile of scaffold-based BMP-2 delivery.

INTRODUCTION

The use of bone morphogenetic proteins (BMPs) for repair of large bone defects is one of the few protein-based tissue engineering strategies that are currently in widespread clinical use. Delivery of exogenous BMPs has been shown to stimulate cellular pathways responsible for osteogenesis and to promote bone formation in both animals and humans (*1*–*3*). The use of clinical products containing recombinant human BMP-2 rose sharply after their introduction into the health care market in 2002, with BMP-2 use accounting for 25% of all spinal fusion surgeries by 2006 (*4*, *5*). Since then, both on-label and off-label applications of BMP-2 have increased, with off-label applications estimated to account for 85% of principle procedures (*5*).

Despite its efficacy in inducing bone formation, clinical BMP-2 delivery has also been associated with numerous complications, including soft tissue inflammation and abnormal (heterotopic) ossification, in as many as 28% of patients treated with BMP-2 for off-label spinal applications (*6*, *7*). These complications are believed to be caused by the supraphysiological doses of BMP-2 that must be used in humans for effective treatment to overcome the short half-life and rapid clearance of the protein in vivo (~6.7 min) (*8*). Clinical doses of BMP-2 typically range from 0.1 to 0.5 mg BMP-2/kg body weight, although off-label use of doses as high as 1 mg BMP-2/kg body weight has also been reported (*7*, *9*).

Given the rapid clearance of BMP-2 from the body, clinical BMP-2 delivery commonly involves adsorption to a collagen sponge scaffold to localize the protein to the bone defect site (*10*, *11*). However, numerous studies have demonstrated that the collagen sponge does not have specific affinity for BMP-2, has no positive impact on its bioactivity, cannot effectively retain the protein within its matrix (<10%), and may even inhibit fracture healing when delivered without BMP-2 (*11*–*14*). Consequently, substantial research has focused on developing more suitable biomaterials to improve BMP-2 stability and retention in vivo.

Hydrogels have been investigated extensively for BMP-2 delivery due to their injectability, amenability to chemical modification to tune material degradation and protein release, and capacity for cell and macromolecule infiltration (*15*). BMP-2 has been immobilized onto fibrin (*13*), polyethylene glycol (*16*), collagen/gelatin (*17*), hyaluronic acid (*12*), and alginate (*18*) using covalent tethering strategies or nonspecific, electrostatic interactions. However, covalent tethering often requires chemical modification of the protein itself, which may result in decreased bioactivity (*19*, *20*), while weak, electrostatic interactions can be easily disrupted in the protein-rich in vivo injury environment (*21*).

BMP-2 delivery can be more precisely controlled by incorporating natural or synthetic BMP-2–binding ligands into the polymer matrix and relying on affinity interactions to control the rate of protein release. Heparin, a naturally occurring glycosaminoglycan with strong affinity for BMP-2 [K_d (dissociation constant) = 20 nM] (*1*), as well as heparin derivatives, has been incorporated into biomaterials to prolong BMP-2 release in vitro and in vivo (*13*, *22*–*25*) and has the added benefit of enhancing BMP-2 bioactivity (*26*, *27*). Similarly, heparin-binding peptides have been used in delivery systems to sequester endogenous heparin and leverage BMP-2–heparin binding (*28*, *29*). Synthetic binding ligands have also been designed to mimic interactions between BMP-2 and extracellular matrix molecules such as fibrin and fibronectin and have exhibited superior BMP-2 binding and controlled delivery in vivo (*30*, *31*). While affinity-controlled release systems for BMP-2 have the potential to improve BMP-2 localization in vivo compared with the clinical collagen sponge, the difficulty of tuning interactions between BMP-2 and its biomimetic ligands may hinder precise growth factor delivery. For example, although incorporating an excess amount of heparin-based microparticles into a hydrogel delivery vehicle decreased BMP-2 release into the surrounding soft tissue, this strategy also inhibited bone formation (*32*). These results highlight the challenge of titrating affinity interactions between BMP-2 and its binding partners.

[1]The Parker H. Petit Institute for Bioengineering and Bioscience, Georgia Institute of Technology, Atlanta, GA 30322, USA. [2]The Knight Campus for Accelerating Scientific Impact, University of Oregon, Eugene, OR 97403, USA. [3]The Gladstone Institute of Cardiovascular Disease, San Francisco, CA 94158, USA. [4]Department of Bioengineering and Therapeutic Sciences, University of California San Francisco, San Francisco, CA 94158, USA.
*Corresponding author. Email: guldberg@uoregon.edu

We have developed microparticles made entirely of cross-linked heparin methacrylamide, which enable high-density growth factor sequestration. These heparin microparticles (HMPs) bind >1000 times more BMP-2 than other previously reported heparin materials (~300 μg BMP-2/mg HMPs) and enhance the potency and half-life of bound BMP-2 beyond that of soluble heparin by facilitating efficient, local growth factor–cell interactions (*23*, *32*). The extremely high BMP-2–binding capacity of HMPs makes them an ideal delivery vehicle for the supraphysiological BMP-2 doses required in the clinic.

In this study, we investigated the efficacy of a composite biomaterial vehicle for sustained BMP-2 delivery to a critically sized femoral defect, in which different amounts of HMPs were incorporated into an alginate hydrogel surrounded by a perforated poly(caprolactone) (PCL) nanofiber mesh. A slow-degrading, PCL nanofiber mesh was used to contain the alginate hydrogel within the defect space during the time frame of bone formation while facilitating robust early cell and tissue infiltration through the mesh pores (*18*). Arginine-glycine-aspartic acid (RGD)–functionalized, calcium–cross-linked alginate was chosen as the vehicle for HMP and BMP-2 delivery, as it enables cell attachment and infiltration, can be degraded hydrolytically, can enhance growth factor activity through transient electrostatic interactions, and has been shown to promote bone formation when loaded with BMP-2 (*18*, *33*–*35*). The ability to cross-link alginate hydrogels with varying amounts of BMP-2–laden HMPs provides the opportunity to easily tune the density of spatial BMP-2 presentation and effective BMP-2 release into the surrounding tissue. Given the challenge of determining the most important parameters affecting BMP-2 release and the most relevant HMP concentrations for in vivo investigation, a computational model was developed to predict the effects of HMP incorporation and other material properties on BMP-2 release.

We used a clinically relevant rodent model, in which high doses of BMP-2 (0.12 mg BMP-2/kg body weight) were delivered to a critically sized, load-bearing bone, and in which characteristic heterotopic ossification has been observed using both alginate and collagen sponge delivery vehicles (*21*, *36*). We hypothesized that HMPs could be used to dose-dependently localize BMP-2 release within the defect site and improve the spatial distribution of bone formation following treatment with high doses of BMP-2.

RESULTS

HMPs maintain BMP-2 bioactivity

To test the reproducibility and functionality of HMP fabrication, 10 batches of HMPs fabricated by free radical cross-linking of six batches of heparin methacrylamide were evaluated for their ability to bind bioactive BMP-2 (Fig. 1 and fig. S1). HMP morphology was similar between batches (fig. S1A), and each batch of HMPs depleted ~70 to 85% of the added BMP-2 (fig. S1B). BMP-2–loaded HMPs induced alkaline phosphatase (ALP) activity in C2C12 cells, demonstrating bioactivity (fig. S1C); all but one of the BMP-2–loaded HMP batches stimulated similar or greater ALP activity compared with soluble BMP-2 treatment. BMP-2–loaded HMPs also increased C2C12 DNA content compared with soluble BMP-2 treatment (fig. S1D), as previously observed (*23*).

HMPs are predicted to increase BMP-2 retention in silico

Varying the number of HMPs delivered, and hence the number of BMP-2 binding sites, was expected to alter the release of BMP-2 from

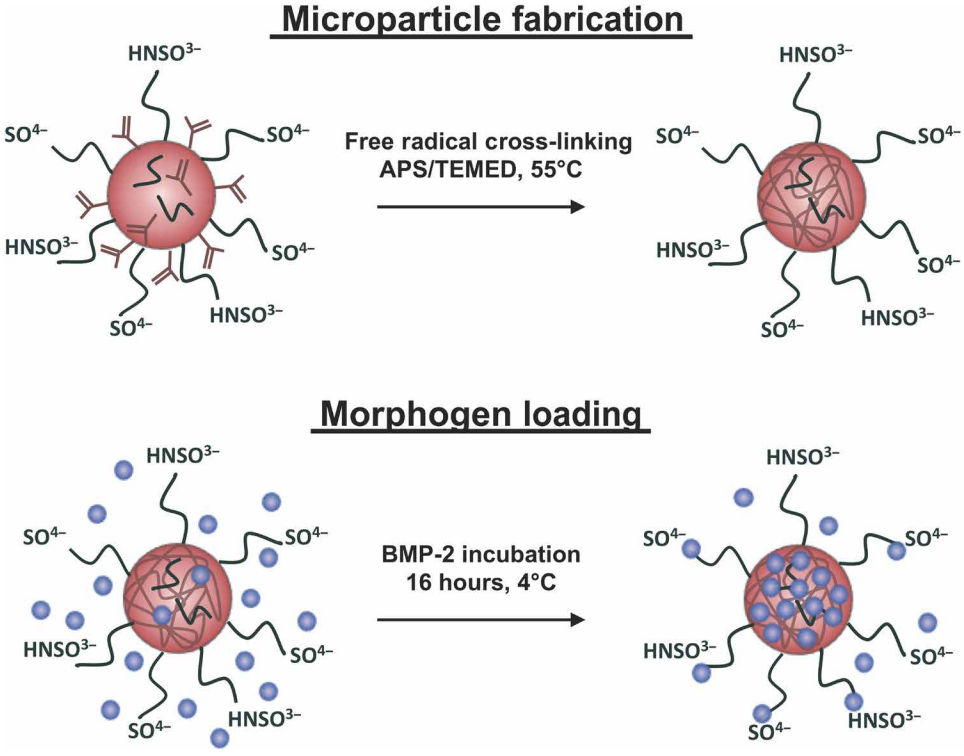

Fig. 1. Fabrication and morphogen loading of HMPs. HMPs were fabricated from heparin methacrylamide using the free radical initiators ammonium persulfate (APS) and *N*,*N*,*N*′,*N*′-tetramethylethane-1,2-diamine (TEMED) in a water-in-oil emulsion at 55°C. BMP-2 was loaded onto HMPs by incubating BMP-2 and HMPs together at 4°C for 16 hours. BMP-2 binds to the sulfate groups on heparin.

the defect site. Thus, a computational model was developed using COMSOL Multiphysics Software to predict BMP-2 release from alginate/PCL constructs containing different amounts of HMPs and 30 μg of BMP-2 (Fig. 2). A sensitivity analysis was run on several key parameters used in the COMSOL model, including the dissociation constant of BMP-2 binding to HMPs (K_d), BMP-2 diffusion coefficient through tissue ($D_{BMP,\ Tissue}$), and BMP-2 diffusion coefficient through alginate ($D_{BMP,\ Alginate}$) (Fig. 2A). K_d, $D_{BMP,\ Tissue}$, and $D_{BMP,\ Alginate}$ were varied by ±2.5 to 10 times their original values, and BMP-2 release into surrounding tissue was changed from 13% to 4–35%, 5–29%, and 12–13%, respectively (Fig. 2B). Thus, overall BMP-2 release was expected to be governed primarily by the dissociation kinetics of BMP-2 from HMPs and the diffusion of BMP-2 through the surrounding tissue. The results of the COMSOL model motivated us to vary the number of HMPs in the construct by orders of magnitude (e.g., 0, 0.01, 0.1, and 1 mg) instead of targeting other less influential parameters (i.e., BMP-2 diffusion coefficient through the hydrogel) to modulate BMP-2 release.

Visual representations of predicted BMP-2 release in the femur at 14 days after injury (Fig. 2C), as well as volume fraction analyses of BMP-2 in the alginate, HMPs, and tissue over time (Fig. 2D), depict attenuated BMP-2 release in the presence of increasing amounts of HMPs. In the absence of HMPs, 87% of the BMP-2 delivered in the tissue-engineered construct was predicted to be released into the surrounding tissue over 14 days (Fig. 2, C and D, iv). Conversely, when BMP-2 delivery was simulated using 1 mg of HMPs, >99% of the BMP-2 was predicted to remain bound to the HMPs after 14 days, with only 0.3% (90 ng) of the BMP-2 entering the surrounding tissue (Fig. 2, C and D, i). This was likely due to the large excess of HMP binding sites compared with BMP-2 molecules (7.0×10^{15} sites and 6.96×10^{14} BMP-2 molecules) and strong affinity between BMP-2 and HMPs (K_d = 50 nM).

When the number of HMPs in the system was reduced 10-fold to 0.1 mg, yielding similar numbers of BMP-2 binding sites and BMP-2 molecules (7.0×10^{14} sites and 6.96×10^{14} molecules), the predicted amount of BMP-2 leaving the construct over 14 days increased to

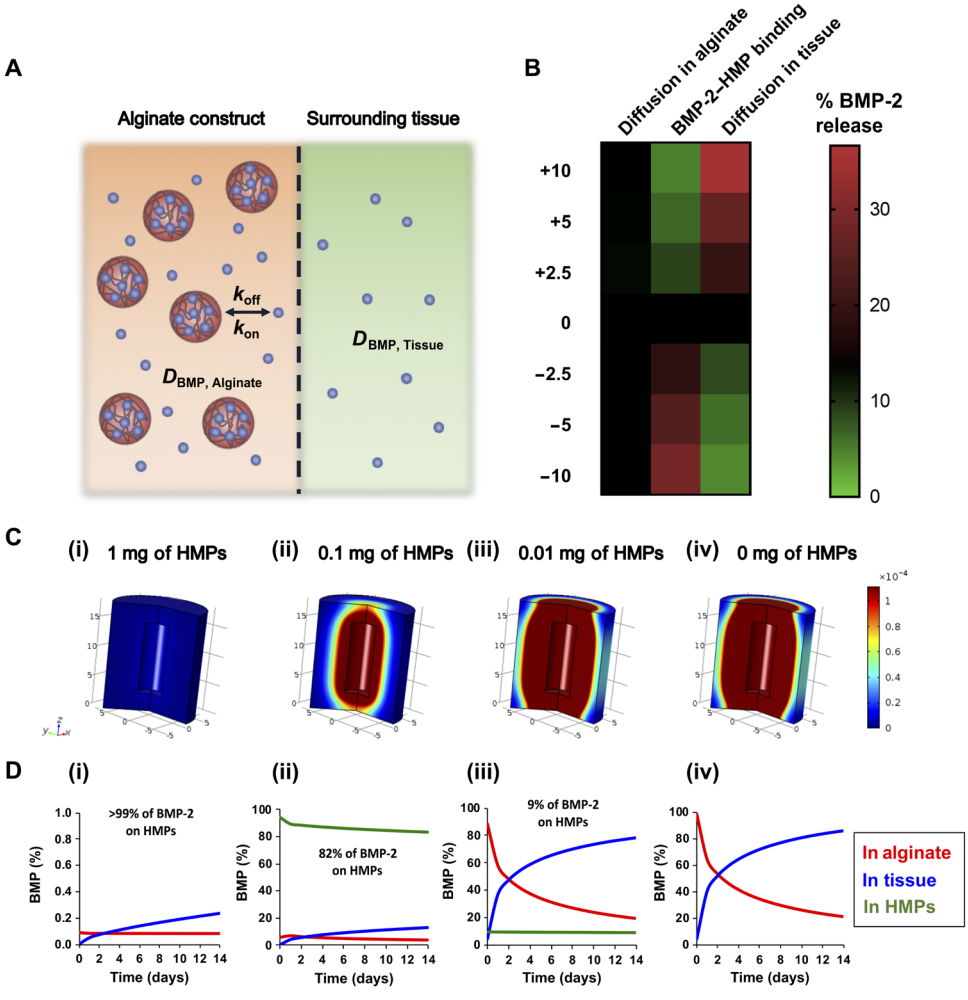

Fig. 2. In silico assessment of BMP-2 release from alginate/PCL tissue-engineered constructs. (**A**) BMP-2 unbinds from HMPs at a rate of k_{off}, rebinds to HMPs at a rate of k_{on}, and diffuses through the alginate hydrogel and surrounding tissue at diffusion rates of $D_{BMP,\ Alginate}$ and $D_{BMP,\ Tissue}$, respectively. (**B**) Heat map depicting the sensitivity of BMP-2 release into surrounding tissue to ±2.5-, 5-, and 10-fold changes in key parameter values. (**C**) Three-dimensional representations of BMP-2 release from tissue-engineered constructs into surrounding soft tissue at 14 days after injury. (**D**) Volume fraction analysis of BMP-2 in alginate hydrogel (red line), in surrounding tissue (blue line), and bound to HMPs (green line). Treatment groups are as follows: (**i**) 30 μg of BMP-2 + 1 mg of HMPs in alginate, (**ii**) 30 μg of BMP-2 + 0.1 of mg HMPs in alginate, (**iii**) 30 μg of BMP-2 + 0.01 mg of HMPs in alginate, and (**iv**) 30 μg of BMP-2 in alginate.

15% (Fig. 2, C and D, ii). However, a further 10-fold reduction in the amount of HMPs to 0.01 mg resulted in fewer HMP binding sites than BMP-2 molecules (7.0×10^{13} sites and 6.96×10^{14} molecules), and subsequently, the majority of the BMP-2 delivered was predicted to exit the construct (78%), with only 9% remaining bound to the HMPs (Fig. 2, C and D, iii). Thus, delivering 30 μg of BMP-2 using 0.1 to 1 mg of HMPs within the alginate/PCL constructs was predicted to improve BMP-2 localization within the bone defect site and chosen for subsequent in vivo studies.

HMPs increase BMP-2 retention in vivo

Subcutaneously implanted constructs containing HMPs (0.1 or 1 mg) and BMP-2 (2.5 μg) labeled with a near-infrared fluorophore (VivoTag 750) were imaged to evaluate BMP-2 retention in the constructs over 21 days (Fig. 3, A to D). When fluorescent signal was normalized to day 0 values and fit to an exponential decay curve (Fig. 3E), constructs containing 1 mg of HMPs exhibited a lower average decay constant than constructs without HMPs, indicating prolonged BMP-2 retention (Fig. 3F). After 21 days in vivo, all constructs exhibited similar BMP-2 retention (16 to 23%). However, when constructs were explanted and imaged ex vivo, the final radiant efficiency measured in constructs containing 1 mg of HMPs was 15% higher than that of constructs containing 0.1 mg of HMPs and 20% higher than that of constructs lacking HMPs (Fig. 3G).

HMPs improve spatial distribution of bone formation in bone defects

Eight-millimeter critically sized femoral defects were treated with hydrogels containing (i) 30 μg of BMP-2 without HMPs, (ii) 30 μg of BMP-2 loaded onto 0.1 mg of HMPs, or (iii) 30 μg of BMP-2 loaded onto 1 mg of HMPs. Longitudinal radiographs revealed progressive bone formation in and around the bone defect in all groups (Fig. 4). Bony bridging was achieved in almost all femurs after 12 weeks (BMP-2: 12 of 14 defects; BMP-2 + 0.1 mg of HMPs: 12 of 13 defects; BMP-2 + 1 mg of HMPs: 13 of 14 defects). Constructs containing BMP-2 alone induced variable bone formation in and around the defect space, and thus, two sets of radiographs representative of the range of heterotopic ossification observed have been included.

Micro–computed tomography (micro-CT) scans, segmented as shown in Fig. 5A, provided quantification of total bone volume (Fig. 5B), heterotopic bone volume (Fig. 5C), and defect bone volume (Fig. 5D) over time. The PCL nanofiber mesh (6-mm diameter), slightly larger than the diameter of the exposed bone ends, was used to demarcate the boundary between defect and heterotopic bone (Fig. 5A). In femurs treated with BMP-2 alone, 65.8 ± 5.3% of the total bone volume was located outside of the defect space 4 weeks after surgery, whereas this amount was decreased to 39.4 ± 5.9% and 44.8 ± 7.9% with treatment with 0.1 mg and 1 mg of HMPs, respectively. At the end of the study, femurs treated with BMP-2 alone still displayed almost twice as much heterotopic bone than femurs treated with BMP-2–loaded HMPs. Despite differences observed in the spatial distribution of mineralization between femoral defects treated with BMP-2 or BMP-2–loaded HMPs, no differences were observed in either mineral density (fig. S2) or biomechanical properties, including torsional stiffness (Fig. 5E) and maximum torque (Fig. 5F).

Bone morphology in HMP-treated bone defects is similar to BMP-2 treatment alone

Histological sections from femurs isolated 12 weeks after injury were stained with hematoxylin and eosin (H&E), Safranin O/Gill's hematoxylin, or Safranin O/Fast Green (Fig. 6). HMPs were stained red with Safranin O or purple with H&E. HMPs were visible and well distributed in all HMP-treated defects after 12 weeks. Safranin O/Fast Green– and H&E-stained sections from all groups demonstrated similar bone

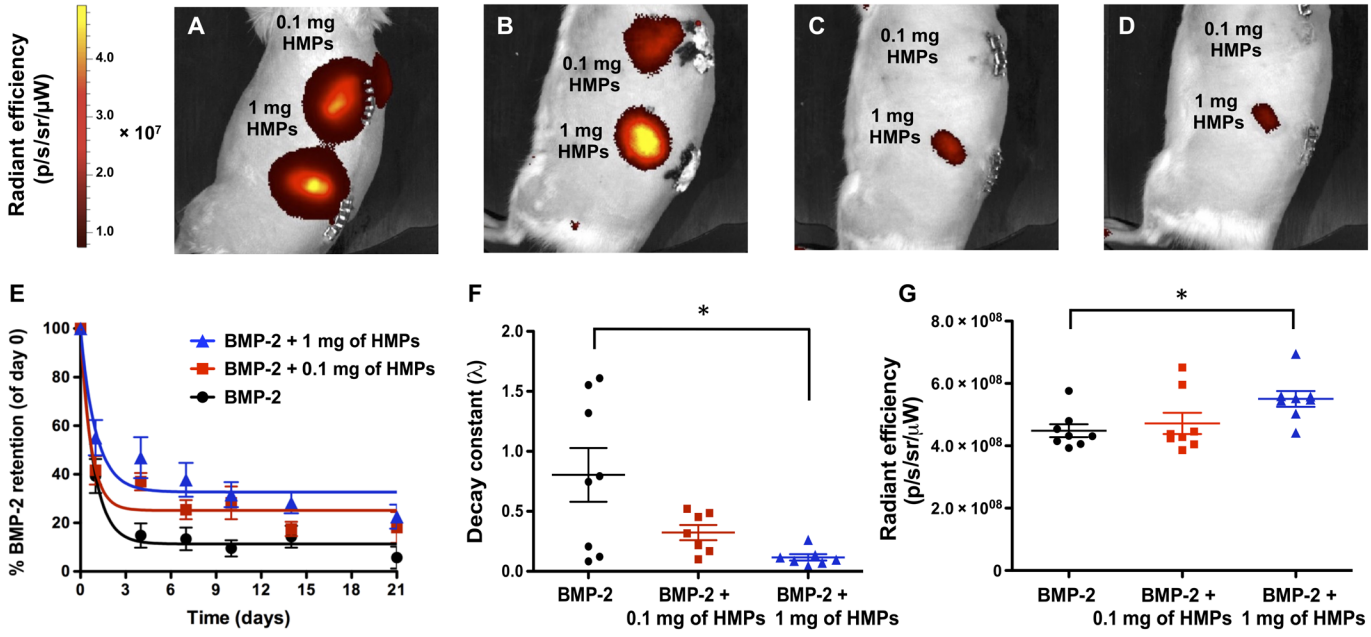

Fig. 3. In vivo tracking of BMP-2 released from alginate/PCL tissue-engineered constructs. (**A** to **D**) Longitudinal IVIS images of constructs containing 2.5 μg of fluorescently labeled BMP-2 loaded onto 0.1 or 1 mg of HMPs at (A) day 0, (B) day 1, (C) day 4, and (D) day 7. (**E**) Quantification of fluorescence within implantation sites and fit to one-phase exponential decay curves ($R^2 = 0.88$ for BMP-2, $R^2 = 0.78$ for BMP-2 + 0.1 mg of HMPs, and $R^2 = 0.68$ for BMP-2 + 1 mg of HMPs.) (**F**) Decay constants obtained from BMP-2 retention curves (*$P < 0.05$ as indicated). (**G**) Radiant efficiency of constructs explanted after 21 days ($n = 7$ to 8; *$P < 0.05$ as indicated).

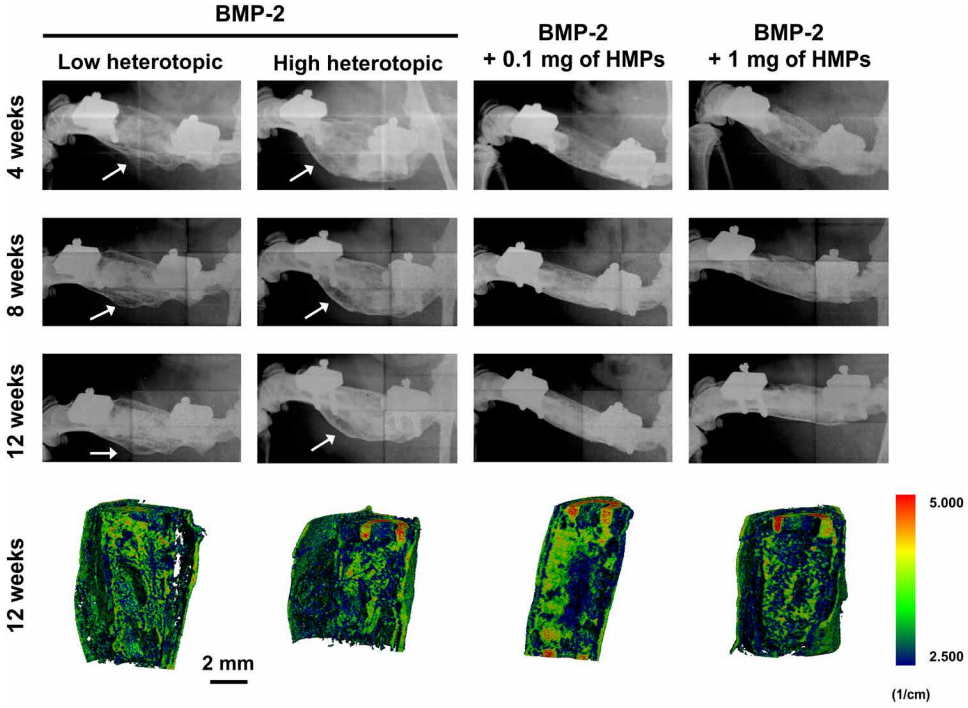

Fig. 4. Representative radiographs and micro-CT reconstructions of femoral defects treated with alginate/PCL tissue-engineered constructs. Constructs contained 30 μg of BMP-2, 30 μg of BMP-2 + 0.1 mg of HMPs, or 30 μg of BMP-2 + 1 mg of HMPs. Radiographs were taken at 4, 8, and 12 weeks. White arrows indicate heterotopic ossification. Mineral density evaluated by micro-CT at 12 weeks is depicted in sagittal sections.

morphology (green in Safranin O/Fast Green and pink in H&E) and areas of residual alginate (orange in Safranin O/Fast Green and purple in H&E). Overall, residual alginate and HMPs appeared to be integrated into larger areas of mineralized tissue.

DISCUSSION

Although robust bone regeneration has been achieved in animal models using a variety of BMP-2 delivery vehicles, these results cannot easily be translated to humans due to the dramatically higher BMP-2 doses required to induce bone repair in humans (0.1 to 1 mg BMP-2/kg body weight) (*7*, *9*)] and do not recapitulate the heterotopic ossification and soft tissue inflammation that are potential consequences of clinical BMP-2 delivery. In addition, challenging conditions typically associated with chronic fracture nonunion in humans cannot easily be treated with low doses of BMP-2 (*37*). The 8-mm rat femoral defect described here exhibits consistent bony bridging following treatment with low BMP-2 doses (0.01 to 0.02 mg BMP-2/kg body weight) delivered within an alginate hydrogel (*18*, *35*). At these low BMP-2 doses, heterotopic ossification and soft tissue inflammation are rare, and therefore, new BMP-2 delivery vehicles have not been developed to address these side effects.

In this study, we leveraged the strong affinity interactions between heparin and BMP-2 to improve sustained delivery of high doses of BMP-2 to a critically sized femoral defect while mitigating heterotopic ossification typically caused by rapid BMP-2 release. Computational modeling of in vivo BMP-2 transport was used to identify parameters that had the largest impact on BMP-2 release in our system and predict doses of HMPs that could modulate BMP-2 release into the surrounding soft tissue. In vivo tracking of BMP-2 release from subcutaneously implanted tissue-engineered constructs revealed prolonged BMP-2 retention in constructs containing HMPs, validating our approach. Femoral defects treated with high BMP-2 doses (0.12 mg BMP-2/kg body weight) loaded onto HMPs exhibited robust local bone formation and low heterotopic ossification, with no negative impacts on bone morphology or biomechanics, demonstrating that HMPs may be used to improve clinically relevant BMP-2 delivery.

Effective BMP-2 delivery for bone repair requires a balance of growth factor release and retention, such that released BMP-2 can act as a chemoattractant to surrounding cells (*38*), and retained BMP-2 can promote bone formation within the defect (*39*). While many delivery vehicles, such as collagen and alginate, provide poor control over BMP-2 localization in vivo, HMPs demonstrate robust BMP-2 binding in vitro, releasing <10% of the loaded protein (*23*) and prolonging BMP-2 bioactivity (*32*). HMP-mediated localization of low doses of BMP-2 (0.01 mg BMP-2/kg body weight) within the bone defect site was previously shown to decrease bone volume compared with alginate delivery of BMP-2 (*32*), suggesting that adequate BMP-2 release was not achieved. Given the marked effect of HMPs on BMP-2 retention in vivo, we sought to explore the use of HMPs for localizing high BMP-2 doses and subsequent bone formation in vivo.

Since the effect of HMPs on BMP-2 release in vivo has previously only been investigated at a single dose (2.5 μg of BMP-2 and 1 mg of HMPs), the effect of HMPs on the delivery of high BMP-2 doses was initially explored in silico. HMPs were predicted to dose-dependently increase BMP-2 retention in the defect, with ≥0.1 mg of HMPs drastically changing the release profile into surrounding tissue compared with delivery in alginate alone, and thus warranting in vivo investigation. Delivery of 5 μg of BMP-2 in alginate has previously

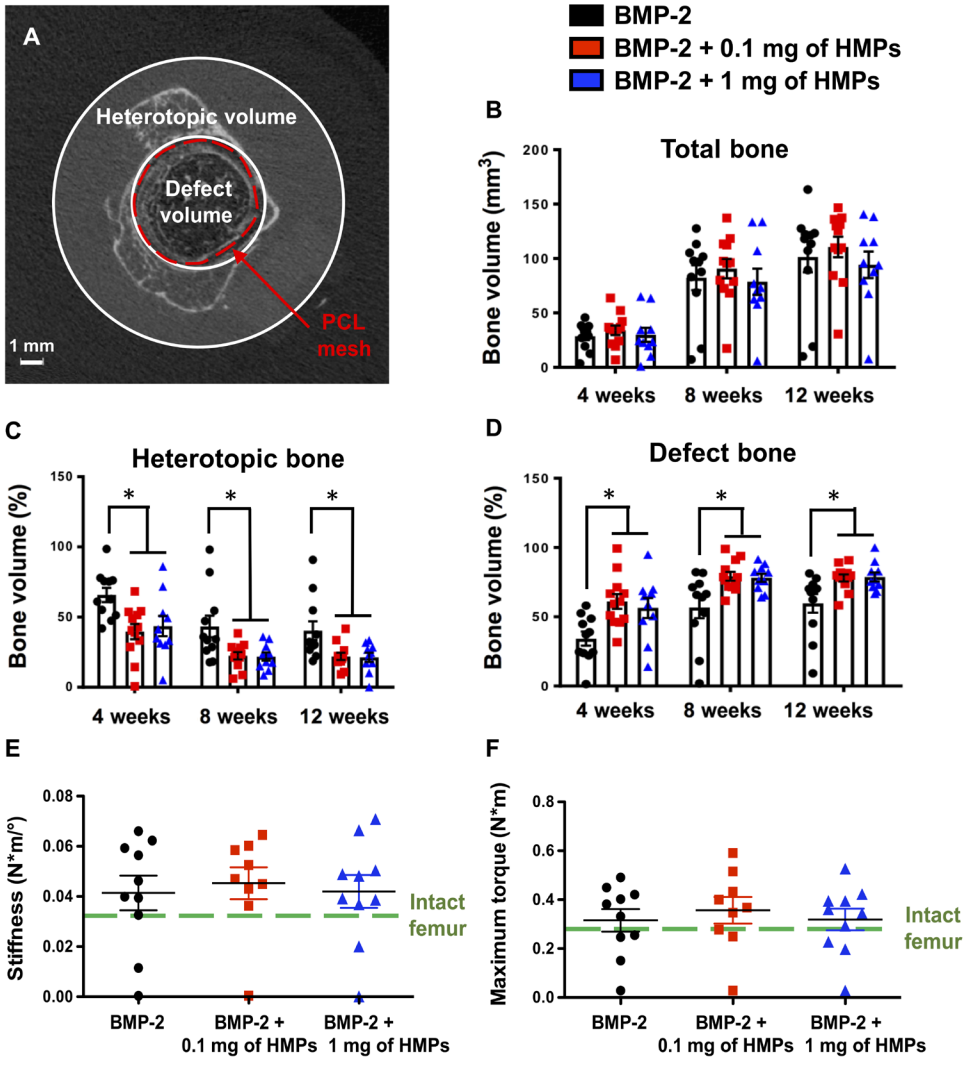

Fig. 5. Quantification of bone volume and biomechanical properties of femoral defects treated with alginate/PCL tissue-engineered constructs. (**A**) Representative micro-CT slice demonstrating that bone volume was divided into defect volume and heterotopic volume based on 6-mm circular contours defined by the PCL nanofiber mesh. (**B**) Total bone volume at 4, 8, and 12 weeks was divided into (**C**) percentage of heterotopic bone volume and (**D**) percentage of defect bone volume (n = 13 to 14; *P < 0.05 as indicated). Excised femurs underwent torsion testing at 12 weeks after injury to calculate (**E**) stiffness and (**F**) maximum torque of regenerated bone. Mechanical properties were compared to that of intact femurs (n = 9 to 10).

exhibited robust bone formation in this animal model, suggesting that its release profile promotes cell infiltration and subsequent mineralization (*35*, *40*); delivery of 30 μg of BMP-2 using 0.1 mg of HMPs was predicted to result in high BMP-2 retention and similar BMP-2 release into the surrounding tissue after 14 days (~4 μg).

We demonstrated that BMP-2 release could be tuned in vivo using HMPs, with increasing HMP amounts decreasing the decay constant of protein release. However, only alginate/PCL constructs containing 1 mg of HMPs demonstrated a significantly lower rate of BMP-2 release compared with constructs lacking HMPs, and BMP-2 release in vivo was faster than what was predicted in silico. Although the computational model was developed using parameters determined through in vitro and in vivo experiments (*32*), the idealized in vivo environment simulated by the model may not have captured all of the elements of the system that could accelerate BMP-2 release kinetics, including changes in material properties caused by cell infiltration and early degradation of the alginate hydrogel, interstitial fluid flow, and competitive binding of other proteins to HMPs in the in vivo injury environment, which has previously only been simulated in vitro using fetal bovine serum (FBS) (*21*). A sensitivity analysis of the computational model revealed that order of magnitude changes in input parameters could be required to alter simulated BMP-2 release profiles, further suggesting that additional factors not included in this analysis may play a crucial role. Moreover, although the model simulated BMP-2 binding sites as being evenly distributed through the alginate hydrogel, in reality, individual HMPs would be focal points of many concentrated BMP-2 binding sites; thus, reducing the number of HMPs by 10-fold may have also decreased the probability of BMP-2 molecules rebinding to other HMPs while diffusing through the alginate hydrogel. Thus far, there are few mathematical models of protein release from biomaterials, which mainly focus on predicting in vitro release profiles (*41*, *42*). Future model development could consider additional factors

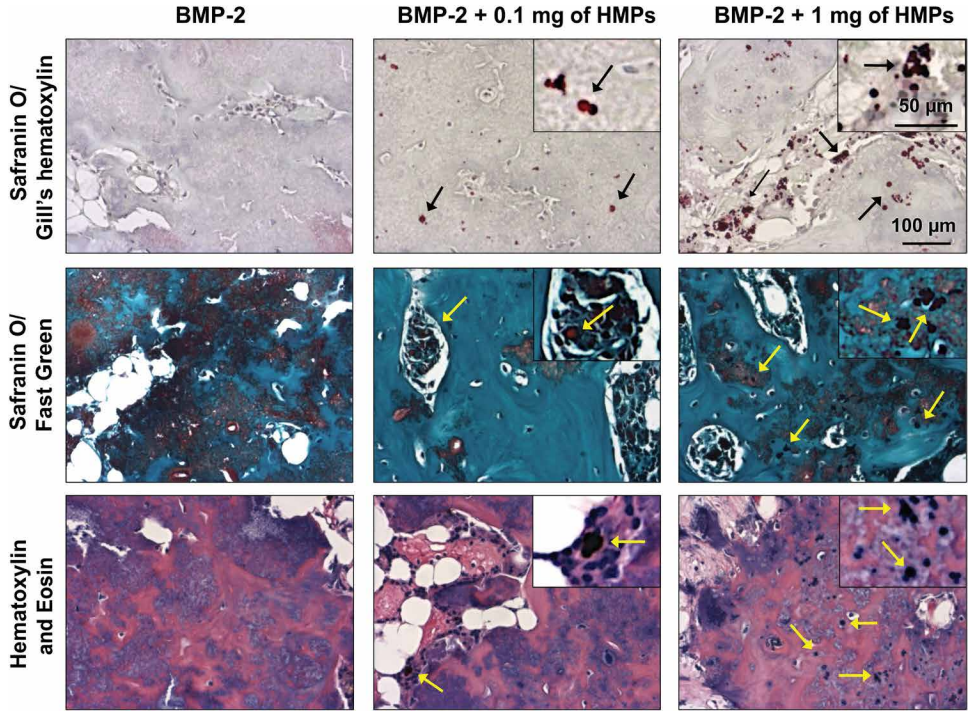

Fig. 6. Femoral bone defect histology at 12 weeks after injury. Femurs were decalcified, paraffin processed, sectioned, and stained with Safranin O/Gill's hematoxylin, Safranin O/Fast Green, or H&E. Black and yellow arrows indicate HMPs.

(hydrogel degradation, interstitial fluid flow, etc.) to more accurately predict BMP-2 release in an in vivo injury environment.

In this study, BMP-2 release was evaluated from constructs implanted subcutaneously. This was motivated, in part, by a previous study, in which comparable release of radiolabeled BMP-2 was observed between scaffolds implanted in subcutaneous and femoral defect environments, with ~50% of the growth factor being released in the first 21 days and detectable signal present for 56 days (*17*). Differences in BMP-2 release profiles between this study and our own may be attributed to the different scaffolds and sensitivity of detection methods used. Furthermore, the differences in cellular and molecular makeup of the implantation sites could have contributed to an altered BMP-2 release profile in the femoral defect environment in our study.

We observed considerable heterotopic bone formation in femoral defects treated with high-dose BMP-2 without HMPs, similar to what has been reported previously in this model (*36*). Previous studies have demonstrated that neither the clinical collagen sponge nor alginate/PCL tissue-engineered construct could mitigate heterotopic ossification at high BMP-2 doses (*36*). However, in this study, the inclusion of 0.1 and 1 mg of HMPs in this tissue-engineered construct markedly reduced heterotopic ossification by 40 and 34% at 4 weeks and by 46 and 47% at 12 weeks, respectively. The proportion of bone within the defect increased correspondingly, and the total bone volume was similar between groups at each time point, indicating that HMPs influenced the spatial distribution of regenerated bone without affecting overall bone volume.

The improvements in BMP-2 release kinetics and mineral distribution caused by HMP delivery did not negatively affect overall bone quality, as indicated by the strength, mineral density, and morphology of regenerated bone. Although more exuberant heterotopic ossification in the femoral defect may be expected to result in higher torsional strength, torsional stiffness and maximum torque were comparable between groups and similar to that of intact femurs. Furthermore, Safranin O/Fast Green and H&E staining demonstrated similar areas of mature bone and cell infiltration in all groups, with no abnormal fibrous tissue or cyst-like structures, which have been observed in rodent and canine models with collagen sponge delivery of high BMP-2 doses (*36*, *43*). Residual alginate was observed in all defects, and intact HMPs were observed in HMP-containing defects; these materials were interspersed between areas of mature bone, suggesting that their slow degradation did not restrict adjacent bone formation.

This study demonstrated a simple method of tuning BMP-2 release from tissue-engineered constructs through the controlled addition of affinity-based interactions between BMP-2 and a heparin-based material. While affinity-controlled release of proteins has been demonstrated in other studies, the dose dependency of growth factor–binding ligand interactions is not often investigated. A similar approach has been reported using the electrostatic interactions between negatively charged poly(lactic-co-glycolic acid) (PLGA) nanoparticles and positively charged growth factors, in which different amounts of PLGA nanoparticles were incorporated into bulk hydrogels, resulting in a dose-dependent delay in growth factor release (*44*). While effective in vitro, this approach relies on predictable degradation of PLGA nanoparticles to control growth factor release, which may be altered in the in vivo injury environment, in which pH and presence of soluble factors could vary over time.

The computational model was crucial in identifying key parameters affecting BMP-2 release and suggested that order of magnitude changes in HMP amounts were necessary to change release rates; however, the range of release profiles observed was not as wide as what was predicted in silico. Furthermore, the spatial distribution of regenerated bone was similar between both HMP-containing groups.

It is possible that a threshold of BMP-2 retention within the defect is needed to reduce heterotopic ossification, and both 0.1 mg and 1 mg of HMPs achieve retention beyond this threshold. This could also be due to a variety of other reasons that warrant future investigation, including that different amounts of HMPs could influence the calcium-mediated cross-linking of the alginate hydrogel and that the density of BMP-2 bound to HMPs may affect protein presentation to cells, which has been previously observed in vitro with skeletal myoblast responses to BMP-2 (*23*). To control for differences in alginate cross-linking and heparin density, equivalent numbers of HMPs with varying heparin content (1 to 10%) could be incorporated into alginate/PCL constructs (*22*).

Previous studies have demonstrated bone formation with the addition of heparin chains into fibrin (*13*), collagen (*45*), alginate (*25*), and PLGA (*24*) scaffolds for BMP-2 delivery. Simple noncovalent adsorption of heparin onto collagen sponge scaffolds did not enhance BMP-2–mediated bone repair (*45*), motivating the use of more complex, covalent heparin immobilization strategies, including 1-ethyl-3-(3-dimethylaminopropyl)carbodiimide (EDC)/*N*-hydroxysuccinimide (NHS) coupling and photo-cross-linking (*24*, *25*). While these strategies have improved BMP-2–mediated bone formation in vivo, none of these studies have extensively investigated the dose dependency of heparin addition to biomaterials on bone formation, which can be easily considered in our system by changing the number of HMPs. It is also unlikely that diffuse heparin chains would confer the same benefits of high-density BMP-2 clustering provided by HMPs. Furthermore, while many heparin-based materials have been used to deliver low BMP-2 doses relevant to rodent models of bone repair, HMPs are the first heparin-based biomaterial investigated for local retention of clinically relevant, supraphysiological doses of BMP-2 and the first heparin-based biomaterial to achieve significant reduction in associated heterotopic ossification.

Ultimately, HMPs present a versatile platform to tune BMP-2 release from a bulk scaffold and can be easily incorporated into other hydrogels at multiple doses. This strategy also allows for the incorporation of HMPs containing different amounts of heparin (1–100%), which can be individually loaded with different heparin-binding proteins, enabling multiple growth factor delivery with tunable release kinetics. Given that the large burst release of BMP-2 from current delivery vehicles is a key limitation hindering the safety and efficacy of clinical BMP-2 treatment, HMPs provide a promising opportunity to improve the safety profile of scaffold-based BMP-2 delivery vehicles, such as the clinically used collagen sponge.

MATERIALS AND METHODS

Study design

The goal of this study was to create a scaffold for BMP-2 delivery that could robustly heal large bone defects while improving spatial localization of the protein and reducing heterotopic ossification. These objectives were addressed by first screening delivery conditions in silico to determine HMP concentrations necessary to improve BMP-2 retention and then demonstrating both improved BMP-2 retention and spatial localization of bone formation in vivo. Sample numbers for each experiment were determined using power analyses of preliminary experiments and are included in the figure legends and table S2. Subcutaneous placement of alginate/PCL constructs was randomized by location, and femoral defect treatments were randomly assigned to each surgeon. Investigators were blinded for all in vivo/ex vivo analyses, including In Vivo Imaging System (IVIS) imaging, micro-CT, x-ray radiography, mechanical testing, and histology.

HMP fabrication and loading

HMPs were fabricated by cross-linking heparin methacrylamide in a water-in-oil emulsion using ammonium persulfate (APS) and *N*,*N*,*N*′,*N*′-tetramethylethane-1,2-diamine (TEMED), as previously described (*23*). Recombinant human BMP-2 (R&D Systems) was labeled with an amine-reactive near-infrared dye (VivoTag 750, PerkinElmer) (*32*). For BMP-2 tracking studies, 0.1 or 1 mg of lyophilized HMPs was mixed with 2.5 μg of fluorescently labeled BMP-2 (R&D Systems) in 25 μl of 0.1% rat serum albumin (RSA) in 4 mM HCl and rotated at 4°C for 16 hours. For bone defect studies, 0.1 or 1 mg of HMPs was loaded with 30 μg of BMP-2 (Pfizer) in a similar manner.

In vitro bioactivity of BMP-2–loaded HMPs

Samples (0.1 mg) of 10 batches of microparticles made from six batches of heparin methacrylamide were loaded with 50 ng of BMP-2 (R&D Systems) to evaluate the consistency of BMP-2 binding. To measure BMP-2 bioactivity, 0.1 mg of unloaded HMPs, 0.1 mg of BMP-2–loaded HMPs, or an equivalent amount of soluble BMP-2 was cultured with skeletal myoblasts (C2C12; 62,500 cells/cm^2) for 72 hours followed by cell lysis. Cell lysate was incubated with *p*-nitrophenyl phosphate to determine ALP activity or fluorescent double-stranded DNA-binding dye (QuantiFluor dsDNA System, Promega) to determine DNA content.

Fluorescence labeling of BMP-2

Recombinant human BMP-2 (R&D Systems) was labeled with a near-infrared fluorophore containing an NHS ester (VivoTag 750, PerkinElmer) for in vivo tracking of BMP-2 release from tissue-engineered constructs. BMP-2 was dissolved in 100 mM $NaPO_4$ at 100 μg/ml and mixed with six times molar excess of VivoTag 750. The reaction proceeded in the dark at room temperature for 4 hours. Excess fluorophore was removed by dialysis using a Slide-A-Lyzer MINI Dialysis Device (Thermo Fisher Scientific) with a 3.5-kDa molecular weight cutoff. Labeled BMP-2 was stored at −80°C.

Tissue-engineered construct fabrication

RGD-functionalized, irradiated alginate [2% (w/v); FMC BioPolymer] was dissolved in equal amounts of α–minimum essential medium (α-MEM) and 0.1% RSA in 4 mM HCl for 4 hours at room temperature (*18*, *32*). HMPs (0.1 or 1 mg) were loaded with 2.5 μg of fluorescently labeled BMP-2 for subcutaneous implantation or 30 μg of BMP-2 for implantation in femoral defects. Then, soluble BMP-2, 0.1 mg of BMP-2–loaded HMPs, or 1 mg of BMP-2–loaded HMPs was mixed into 150 μl of alginate using two 1-ml syringes connected by a Luer-Lock syringe connector (Cole Parmer). Alginate was cross-linked by mixing in a similar manner with excess calcium sulfate (8.4 mg/ml) until the appearance was uniform and stored overnight at 4°C.

PCL nanofiber mesh tubes were fabricated as previously described (*18*, *32*). PCL [12% (w/v)] was dissolved in a 90:10 solution of hexafluoro-2-propanol/ dimethylformamide overnight. Approximately 5 to 6 ml of PCL solution was electrospun onto a static collector covered in aluminum foil, creating a 0.5-mm-thick mesh sheet. Perforated rectangular sheets were laser cut from meshes (12 mm by 19 mm; 0.9-mm-diameter holes), rolled into tubes [4.5 mm (inner diameter) by 12 mm (length)], and glued using an ultraviolet curing adhesive (Dymax,

Torrington, CT). Mesh tubes were disinfected in 70% ethanol and then immersed in α-MEM for at least 16 hours before use.

For subcutaneous implantation, 150 μl of alginate hydrogel containing BMP-2 or BMP-2–loaded HMPs was injected into perforated PCL nanofiber mesh tubes before implantation. For femoral defect implantation, empty mesh tubes were placed in the defect and filled with 150 μl of BMP-2–loaded alginate hydrogel.

BMP-2 release and diffusion model

A computational model of in vivo BMP-2 release from tissue-engineered constructs was developed using COMSOL Multiphysics Software (version 5.2a) (*32*). The three-dimensional bone defect and surrounding tissue were modeled as two nested rectangles in a two-dimensional, axisymmetric modeling domain (Fig. 2A). Thus, the subdomains consisted of (i) the alginate hydrogel within the bone defect and (ii) the surrounding thigh tissue. The reaction engineering physics module was used to model the interactions between BMP-2 and HMPs, while the transport of dilute species physics module was used to model BMP-2 diffusion through the alginate hydrogel and into surrounding tissue. Equations for BMP-2 diffusion and interactions with HMPs were based on Fick's laws of diffusion and simple binding kinetics (*46*) and have been described in our previous publication (*32*).

The parameters used for the COMSOL simulations are described in table S1. The effective diffusion coefficient of BMP-2 through the alginate hydrogel ($D_{BMP,\ Alginate}$) was determined on the basis of in vitro BMP-2 diffusion through 2% (w/v) alginate hydrogels in capillary tubes (*47*). The effective diffusion coefficient of BMP-2 through the perforated nanofiber mesh tube and surrounding tissue ($D_{BMP,\ Tissue}$) was approximated on the basis of fluorescent BMP-2 tracking in the bone defect site (*35*). The number of BMP-2 binding sites on HMPs was calculated using an experimentally determined maximum binding capacity of HMPs (300 μg BMP-2/mg HMPs) (*23*). The release of BMP-2 from HMPs in 100% FBS was used to calculate rate constants to describe BMP-2–HMP interactions in simulated in vivo conditions. Rate constants were initially chosen on the basis of BMP-2 binding to unmodified heparin (K_d = 20 nM, $k_{on} = 5.1 \times 10^{-4}$ 1/nM·s, and k_{off} = 0.01 1/s) (*1*) and subsequently adjusted for HMPs using a COMSOL model of in vitro BMP-2–HMP interactions in FBS (*21*), which revealed that a higher dissociation rate constant than that of unmodified heparin was necessary to accurately model the experimental results (K_d = 50 nM, $k_{on} = 5.1 \times 10^{-4}$ 1/nM·s, and k_{off} = 0.025 1/s).

A sensitivity analysis was performed by varying several critical parameters by ±2.5-, 5-, or 10-fold: (i) the dissociation constant describing BMP-2 and HMP binding, (ii) the diffusion coefficient through tissue, and (iii) the diffusion coefficient through the alginate hydrogel (*47*).

Subcutaneous implant surgery

All surgical procedures were conducted according to the Georgia Institute of Technology Institutional Animal Care and Use Committee protocols. For in vivo BMP-2 tracking studies, alginate/PCL constructs were subcutaneously implanted into the backs of 13-week-old female SASCO Sprague-Dawley rats (Charles River Laboratories) using a metal rod and cannula (four constructs per rat) (*32*). Constructs contained (i) 2.5 μg of labeled BMP-2 in alginate, (ii) 2.5 μg of labeled BMP-2 + 0.1 mg of HMPs in alginate, or (iii) 2.5 μg of labeled BMP-2 + 1 mg of HMPs in alginate.

In vivo BMP-2 tracking

In vivo and ex vivo fluorescence imaging (excitation, 745; emission, 800; 5 s) was performed using an IVIS Spectrum platform (PerkinElmer). Longitudinal in vivo imaging was performed immediately following subcutaneous implantation on day 0, as well as on days 1, 4, 7, 10, 14, and 21. Total fluorescent counts and radiant efficiency were evaluated using a 7-cm^2 elliptical region of interest in Living Image Software (PerkinElmer). Normalized fluorescent signal over time was fit to a one-phase exponential decay equation ($y = ae^{-\lambda x}$) in MATLAB to obtain the decay constant, λ. Constructs were also ex vivo imaged after 21 days.

Femoral defect surgery

Unilateral femoral bone defects were created and treated as previously described in 13-week-old female SASCO Sprague-Dawley rats (*18*). A polysulfone and stainless steel fixation plate was screwed onto the femur of the rat, and an 8-mm-wide, full thickness defect was created using an oscillating saw. A PCL nanofiber mesh tube was placed around the exposed bone ends, and 150 μl of calcium–cross-linked alginate hydrogel, containing (i) 30 μg of BMP-2, (ii) 30 μg of BMP-2 + 0.1 mg of HMPs, or (iii) 30 μg of BMP-2 + 1 mg of HMPs, was injected into the lumen of the mesh tube through perforations in the PCL mesh tube using an 18-gauge (0.84 mm) needle.

Radiography and micro-CT

Longitudinal radiographs were obtained at 4, 8, and 12 weeks after surgery (Faxitron MX-20, 23 kV, 15 s). Micro-CT was performed at 4, 8, and 12 weeks after surgery using a VivaCT40 live animal scanner (Scanco) at medium resolution with a voxel size of 38.5 μm, voltage of 55 kVp, and a current of 109 μA. Mineral was quantified within the central 5.85 mm (152 scan slices) of each 8-mm defect as total bone volume, defect bone volume (6-mm-diameter contours), and heterotopic bone volume. A global threshold for new bone formation was set at 50% of the average mineral density of native cortical bone based on previous studies (*35*, *36*) and visual analysis of multiple CT scan slices to ensure that this threshold captured new bone formation while avoiding detection of the fixation plate, PCL mesh tube, and surrounding soft tissue.

Biomechanical testing

The ends of the femurs were potted in molten Wood's metal (Alfa Aesar) in custom holders, allowed to solidify, and mounted in the test clamps. Torsion was applied at a rate of 3°/s until failure on a uniaxial torsion testing system (EnduraTEC ELF200, Bose), allowing for the determination of maximum torque and calculation of torsional stiffness, using the slope of the linear segment of the torque-rotation curve.

Histology

Representative femurs isolated 12 weeks after surgery were fixed in 10% neutral-buffered formalin at 4°C for 48 hours. Femurs were decalcified and embedded in paraffin wax by HistoTox Labs Inc. Mid-sagittal sections (5 μm) of the defects were stained with Safranin O/Gill's hematoxylin, Safranin O/Fast Green, and H&E.

Statistical analyses

Statistical analyses were performed using GraphPad Prism (version 7.0), and all data are reported as means ± SEM. Statistical significance was determined using one-way or two-way analysis of variance (ANOVA)

as appropriate, followed by Bonferroni's post hoc analysis. For data that did not satisfy the assumptions of equal variances and Gaussian distributions (Fig. 3F), the nonparametric Kruskal-Wallis test was used, followed by Dunn's multiple comparisons test. $P < 0.05$ was considered statistically significant. Normalized fluorescent signal (Fig. 3E) was fit to a one-phase exponential decay equation using MATLAB 2015a.

SUPPLEMENTARY MATERIALS

Supplementary material for this article is available at http://advances.sciencemag.org/cgi/content/full/6/1/eaay1240/DC1

Fig. S1. Reproducibility of HMP fabrication.

Fig. S2. Mineral density of regenerated bone in femoral defects.

Table S1. Parameters used in the COMSOL model of BMP-2 release in femoral defect.

Table S2. Summary of sample numbers for in vivo experiments.

View/request a protocol for this paper from *Bio-protocol*.

REFERENCES AND NOTES

1. R. Ruppert, E. Hoffmann, W. Sebald, Human BMP-2 contains a heparin-binding site which modifies its biological activity. *FEBS J.* **237**, 295–302 (1998).
2. M. R. Urist, A. Mikulski, A. Lietze, Solubilized and insolubilized BMP. *Proc. Natl. Acad. Sci. U.S.A.* **76**, 1828–1832 (1979).
3. S. Govender, C. Csimma, H. K. Genant, A. Valentin-Opran, Y. Amit, R. Arbel, H. Aro, D. Atar, M. Bishay, M. G. Börner, P. Chiron, P. Choong, J. Cinats, B. Courtenay, R. Feibel, B. Geulette, C. Gravel, N. Haas, M. Raschke, E. Hammacher, D. van der Velde, P. Hardy, M. Holt, C. Josten, R. L. Ketterl, B. Lindeque, G. Lob, H. Mathevon, G. McCoy, D. Marsh, R. Miller, E. Munting, S. Oevre, L. Nordsletten, A. Patel, A. Pohl, W. Rennie, P. Reynders, P. M. Rommens, J. Rondia, W. C. Rossouw, P. J. Daneel, S. Ruff, A. Rüter, S. Santavirta, T. A. Schildhauer, C. Gekle, R. Schnettler, D. Segal, H. Seiler, R. B. Snowdowne, J. Stapert, G. Taglang, R. Verdonk, L. Vogels, A. Weckbach, A. Wentzensen, T. Wisniewski; BMP-2 Evaluation in Surgery for Tibial Trauma (BESTT) Study Group, Recombinant human BMP-2 for treatment of open tibial fractures a prospective, controlled, randomized study of four hundred and fifty patients. *J. Bone Joint Surg.* **84**, 2123–2134 (2002).
4. A. W. James, G. LaChaud, J. Shen, G. Asatrian, V. Nguyen, X. Zhang, K. Ting, C. Soo, A review of the clinical side effects of BMP-2. *Tissue Eng. Part B* **22**, 284–297 (2016).
5. K. L. Ong, M. L. Villarraga, E. Lau, L. Y. Carreon, S. M. Kurtz, S. D. Glassman, Off-label use of BMPs in the United States using administrative data. *Spine* **35**, 1794–1800 (2010).
6. J. D. Smucker, J. M. Rhee, K. Singh, S. T. Yoon, J. G. Heller, Increased swelling complications associated with off-label usage of rhBMP-2 in the anterior cervical spine. *Spine* **31**, 2813–2819 (2006).
7. L. B. Shields, G. H. Raque, S. D. Glassman, M. Campbell, T. Vitaz, J. Harpring, C. B. Shields, Adverse effects associated with high-dose recombinant human BMP-2 use in anterior cervical spine fusion. *Spine* **31**, 542–547 (2006).
8. A. R. Poynton, J. M. Lane, Safety profile for the clinical use of BMPs in the spine. *Spine* **27**, S40–S48 (2002).
9. R. Fu, S. Selph, M. McDonagh, K. Peterson, A. Tiwari, R. Chou, M. Helfand, Effectiveness and harms of recombinant human BMP-2 in spine fusion: A systematic review and meta-analysis. *Ann. Intern. Med.* **158**, 890–902 (2013).
10. M. Geiger, R. H. Li, W. Friess, Collagen sponges for bone regeneration with rhBMP-2. *Adv. Drug Deliv. Rev.* **55**, 1613–1629 (2003).
11. W. Friess, H. Uludag, S. Foskett, R. Biron, C. Sargeant, Characterization of absorbable collagen sponges as rhBMP-2 carriers. *Int. J. Pharm.* **187**, 91–99 (1999).
12. G. Bhakta, Z. X. Lim, B. Rai, T. Lin, J. H. Hui, G. D. Prestwich, A. J. Van Wijnen, V. Nurcombe, S. M. Cool, The influence of collagen and hyaluronan matrices on the delivery and bioactivity of BMP-2 and ectopic bone formation. *Acta Biomater.* **9**, 9098–9106 (2013).
13. H. S. Yang, W.-G. La, Y.-M. Cho, W. Shin, G.-D. Yeo, B.-S. Kim, Comparison between heparin-conjugated fibrin and collagen sponge as BMP-2 carriers for bone regeneration. *Exp. Mol. Med.* **44**, 350–355 (2012).
14. A. Lang, M. Kirchner, J. Stefanowski, M. Durst, M.-C. Weber, M. Pfeiffenberger, A. Damerau, A. E. Hauser, P. Hoff, G. N. Duda, Collagen I-based scaffolds negatively impact fracture healing in a mouse osteotomy model although used routinely in research and clinical application. *Acta Biomater.* **86**, 171–184 (2019).
15. P. S. Lienemann, M. P. Lutolf, M. Ehrbar, Biomimetic hydrogels for controlled biomolecule delivery to augment bone regeneration. *Adv. Drug Deliv. Rev.* **64**, 1078–1089 (2012).
16. A. Shekaran, J. R. García, A. Y. Clark, T. E. Kavanaugh, A. S. Lin, R. E. Guldberg, A. J. García, Bone regeneration using an α 2 β 1 integrin-specific hydrogel as a BMP-2 delivery vehicle. *Biomaterials* **35**, 5453–5461 (2014).
17. D. H. Kempen, L. Lu, A. Heijink, T. E. Hefferan, L. B. Creemers, A. Maran, M. J. Yaszemski, W. J. Dhert, Effect of local sequential VEGF and BMP-2 delivery on ectopic and orthotopic bone regeneration. *Biomaterials* **30**, 2816–2825 (2009).
18. Y. M. Kolambkar, K. M. Dupont, J. D. Boerckel, N. Huebsch, D. J. Mooney, D. W. Hutmacher, R. E. Guldberg, An alginate-based hybrid system for growth factor delivery in the functional repair of large bone defects. *Biomaterials* **32**, 65–74 (2011).
19. M. H. Hettiaratchi, M. J. O'Meara, C. J. Teal, S. L. Payne, A. J. Pickering, M. S. Shoichet, Local delivery of stabilized chondroitinase abc degrades chondroitin sulfate proteoglycans in stroke-injured rat brains. *J. Control. Release* **297**, 14–25 (2019).
20. J. A. Shadish, G. M. Benuska, C. A. DeForest, Bioactive site-specifically modified proteins for 4D patterning of gel biomaterials. *Nat. Mater.* , (2019).
21. M. H. Hettiaratchi, C. Chou, N. Servies, J. M. Smeekens, A. Cheng, C. Esancy, R. Wu, T. C. McDevitt, R. E. Guldberg, L. Krishnan, Competitive protein binding influences heparin-based modulation of spatial growth factor delivery for bone regeneration. *Tissue Eng. Part A* **23**, 683–695 (2017).
22. L. E. Tellier, T. Miller, T. C. McDevitt, J. S. Temenoff, Hydrolysis and sulfation pattern effects on release of bioactive BMP-2 from heparin-based microparticles. *J. Mater. Chem. B* **3**, 8001–8009 (2015).
23. M. H. Hettiaratchi, T. Miller, J. S. Temenoff, R. E. Guldberg, T. C. McDevitt, Heparin microparticle effects on presentation and bioactivity of BMP-2. *Biomaterials* **35**, 7228–7238 (2014).
24. O. Jeon, S. J. Song, S.-W. Kang, A. J. Putnam, B.-S. Kim, Enhancement of ectopic bone formation by BMP-2 released from a heparin-conjugated poly(l-lactic-co-glycolic acid) scaffold. *Biomaterials* **28**, 2763–2771 (2007).
25. O. Jeon, C. Powell, L. D. Solorio, M. D. Krebs, E. Alsberg, Affinity-based growth factor delivery using biodegradable, photocrosslinked heparin-alginate hydrogels. *J. Control. Release* **154**, 258–266 (2011).
26. B. Zhao, T. Katagiri, H. Toyoda, T. Takada, T. Yanai, T. Fukuda, U.-i. Chung, T. Koike, K. Takaoka, R. Kamijo, Heparin potentiates the in vivo ectopic bone formation induced by BMP-2. *J. Biol. Chem.* **281**, 23246–23253 (2006).
27. D. S. Bramono, S. Murali, B. Rai, L. Ling, W. T. Poh, Z. X. Lim, G. S. Stein, V. Nurcombe, A. J. van Wijnen, S. M. Cool, Bone marrow-derived heparan sulfate potentiates the osteogenic activity of bone morphogenetic protein-2 (BMP-2). *Bone* **50**, 954–964 (2012).
28. S. S. Lee, B. J. Huang, S. R. Kaltz, S. Sur, C. J. Newcomb, S. R. Stock, R. N. Shah, S. I. Stupp, Bone regeneration with low dose BMP-2 amplified by biomimetic supramolecular nanofibers within collagen scaffolds. *Biomaterials* **34**, 452–459 (2013).
29. G. A. Hudalla, N. A. Kouris, J. T. Koepsel, B. M. Ogle, W. L. Murphy, Harnessing endogenous growth factor activity modulates stem cell behavior. *Integr. Biol.* **3**, 832–842 (2011).
30. M. M. Martino, P. S. Briquez, A. Ranga, M. P. Lutolf, J. A. Hubbell, Heparin-binding domain of fibrin (ogen) binds growth factors and promotes tissue repair when incorporated within a synthetic matrix. *Proc. Natl. Acad. Sci. U.S.A.* **110**, 4563–4568 (2013).
31. M. M. Martino, F. Tortelli, M. Mochizuki, S. Traub, D. Ben-David, G. A. Kuhn, R. Müller, E. Livne, S. A. Eming, J. A. Hubbell, Engineering the growth factor microenvironment with fibronectin domains to promote wound and bone tissue healing. *Sci. Transl. Med.* **3**, 100ra89 (2011).
32. M. H. Hettiaratchi, T. Rouse, C. Chou, L. Krishnan, H. Y. Stevens, M.-T. A. Li, T. C. McDevitt, R. E. Guldberg, Enhanced in vivo retention of low dose BMP-2 via heparin microparticle delivery does not accelerate bone healing in a critically sized femoral defect. *Acta Biomater.* **59**, 21–32 (2017).
33. E. Alsberg, K. Anderson, A. Albeiruti, R. Franceschi, D. Mooney, Cell-interactive alginate hydrogels for bone tissue engineering. *J. Dent. Res.* **80**, 2025–2029 (2001).
34. M. C. Peters, B. C. Isenberg, J. A. Rowley, D. J. Mooney, Release from alginate enhances the biological activity of vascular endothelial growth factor. *Aust. J. Biol. Sci.* **9**, 1267–1278 (1998).
35. J. D. Boerckel, Y. M. Kolambkar, K. M. Dupont, B. A. Uhrig, E. A. Phelps, H. Y. Stevens, A. J. García, R. E. Guldberg, Effects of protein dose and delivery system on BMP-mediated bone regeneration. *Biomaterials* **32**, 5241–5251 (2011).
36. L. Krishnan, L. B. Priddy, C. Esancy, B. S. Klosterhoff, H. Y. Stevens, L. Tran, R. E. Guldberg, Delivery vehicle effects on bone regeneration and heterotopic ossification induced by high dose BMP-2. *Acta Biomater.* **49**, 101–112 (2017).
37. A. Cheng, L. Krishnan, P. Pradhan, L. D. Weinstock, L. B. Wood, K. Roy, R. E. Guldberg, Impaired bone healing following treatment of established nonunion correlates with serum cytokine expression. *J. Orthop. Res.* **37**, 299–307 (2018).
38. J. Fiedler, G. Röderer, K. P. Günther, R. E. Brenner, BMP-2, BMP-4, and PDGF-bb stimulate chemotactic migration of primary human mesenchymal progenitor cells. *J. Cell. Biochem.* **87**, 305–312 (2002).
39. D. Chen, M. Harris, G. Rossini, C. Dunstan, S. Dallas, J. Feng, G. Mundy, S. Harris, BMP-2 enhances BMP-3, BMP-4, and bone cell differentiation marker gene expression during the induction of mineralized bone matrix formation in culturesof fetal rat calvarial osteoblasts. *Calcif. Tissue Int.* **60**, 283–290 (1997).

40. J. D. Boerckel, Y. M. Kolambkar, H. Y. Stevens, A. S. Lin, K. M. Dupont, R. E. Guldberg, Effects of in vivo mechanical loading on large bone defect regeneration. *J. Orthop. Res.* **30**, 1067–1075 (2012).
41. D. J. Maxwell, B. C. Hicks, S. Parsons, S. E. Sakiyama-Elbert, Development of rationally designed affinity-based drug delivery systems. *Acta Biomater.* **1**, 101–113 (2005).
42. K. Vulic, M. M. Pakulska, R. Sonthalia, A. Ramachandran, M. S. Shoichet, Mathematical model accurately predicts protein release from an affinity-based delivery system. *J. Control. Release* **197**, 69–77 (2015).
43. M. F. Sciadini, K. D. Johnson, Evaluation of recombinant human BMP-2 as a bone-graft substitute in a canine segmental defect model. *J. Orthop. Res.* **18**, 289–302 (2000).
44. M. M. Pakulska, I. E. Donaghue, J. M. Obermeyer, A. Tuladhar, C. K. McLaughlin, T. N. Shendruk, M. S. Shoichet, Encapsulation-free controlled release: Electrostatic adsorption eliminates the need for protein encapsulation in PLGA nanoparticles. *Sci. Adv.* **2**, e1600519 (2016).
45. M. R. Johnson, J. D. Boerckel, K. M. Dupont, R. E. Guldberg, Functional restoration of critically sized segmental defects with BMP-2 and heparin treatment. *Clin. Orthop. Relat. Res.* **469**, 3111–3117 (2011).
46. J. Crank, *The mathematics of diffusion* (Oxford University Press, 1979).
47. M. H. Hettiaratchi, A. Schudel, T. Rouse, A. J. García, S. N. Thomas, R. E. Guldberg, T. C. McDevitt, A rapid method for determining protein diffusion through hydrogels for regenerative medicine applications. *APL Bioeng.* **2**, 026110 (2018).

Acknowledgments: We thank R. Akman, O. Burnsed, L. M. Castro, A. Cheng, B. Klosterhoff, A. Lam, K. Parchinski, D. Reece, M. Ruehle, G. Salazar-Noratto, H. Stevens, B. Torstrick, and J. Wang for assistance with surgeries. **Funding:** This work was supported by funding from the NIH (R01 AR062006 to T.C.M.) and the Armed Forces Institute of Regenerative Medicine (award W81XWH-14-2-0003 to R.E.G.). The U.S. Army Medical Research Acquisition Activity is the awarding and administering acquisition office. Opinions, interpretations, conclusions, and recommendations are those of the authors and are not necessarily endorsed by the Department of Defense. M.H.H. was supported by a Natural Sciences and Engineering Research Council of Canada (NSERC) postgraduate scholarship and Philanthropic Educational Organization (P.E.O.) Scholar Award. C.C. was supported by the Petit Undergraduate Research Scholars Program at Georgia Tech. **Author contributions:** M.H.H., L.K., T.C.M., and R.E.G. designed the research. M.H.H., L.K., and C.C. performed the research. T.R. contributed new analytic tools. M.H.H. analyzed the data. M.H.H., L.K., T.C.M., and R.E.G. wrote the paper. **Competing interests:** The authors declare that they have no competing interests. **Data and materials availability:** All data needed to evaluate the conclusions in the paper are present in the paper and/or the Supplementary Materials. Additional data related to this paper may be requested from the authors.

Submitted 22 May 2019
Accepted 7 November 2019
Published 3 January 2020
10.1126/sciadv.aay1240

Citation: M. H. Hettiaratchi, L. Krishnan, T. Rouse, C. Chou, T. C. McDevitt, R. E. Guldberg, Heparin-mediated delivery of bone morphogenetic protein-2 improves spatial localization of bone regeneration. *Sci. Adv.* **6**, eaay1240 (2020).

Science Advances

Heparin-mediated delivery of bone morphogenetic protein-2 improves spatial localization of bone regeneration

Marian H. Hettiaratchi, Laxminarayanan Krishnan, Tel Rouse, Catherine Chou, Todd C. McDevitt and Robert E. Guldberg

Sci Adv **6** (1), eaay1240.
DOI: 10.1126/sciadv.aay1240